ARE THERE BOUND η-MESONS?*

H. Machner

Fakultät für Physik, Universität Duisburg-Essen
Lotharstr. 1, 47048 Duisburg, Germany
hartmut.machner@uni-due.de

(Received January 7, 2014)

The η meson can be bound to atomic nuclei. Experimental search is discussed in the form of final state interaction for the reactions $dp \to {}^3\mathrm{He}\eta$ and $dd \to {}^4\mathrm{He}\eta$. For the latter case, tensor polarized deuterons were used in order to extract the s-wave strength. For both reactions, complex scattering lengths are deduced: $a_{^3\mathrm{He}\eta} = \left[\pm\left(10.7 \pm 0.8^{+0.1}_{-0.5}\right) + i\,\left(1.5 \pm 2.6^{+1.0}_{-0.9}\right)\right]$ fm and $a_{^4\mathrm{He}\eta} = [\pm\,(3.1 \pm 0.5) + i\,(0 \pm 0.5)]$ fm. For the reaction $p{}^6\mathrm{Li}{\to}{}^7\mathrm{Be}\eta$, more data in the threshold region are necessary to draw any conclusions. In a two-nucleon transfer reaction under quasi-free conditions, $p{}^{27}\mathrm{Al} \to {}^3\mathrm{He}X$ was investigated. The system X can be the bound ${}^{25}\mathrm{Mg}{\otimes}\eta$ at rest. When a possible decay of an intermediate $N^*(1535)$ is required, a highly significant bump shows up in the missing-mass spectrum. The data give for a bound state a binding energy of 13.3 ± 1.6 MeV and a width of $\sigma = 4.4 \pm 1.3$ MeV.

DOI:10.5506/APhysPolB.45.705
PACS numbers: 21.85.+d, 13.75.–n

1. Introduction

In contrast to the pion–nucleon interaction, the η-nucleon interaction at small momenta is attractive and rather strong. This attraction can be seen from the fact that the η threshold (1488 MeV) is situated just below the $N^*(1535)$ resonance which couples strongly to the η–N channel. Initial calculations by Bhalerao and Liu [1] obtained attractive s-wave η–N scattering lengths. With these values, Haider and Liu [2] have shown that η can be bound in nuclei with $A \geq 10$. Other groups have also found similar results [3–5].

On the experimental side, results are meager. The first experiments searching for η-mesic nuclei at BNL [6] and LAMPF [7] by using a missing-mass technique in the (π^+, p) reaction reached negative or inconclusive results. Later, it became clear that the peaks are not necessarily narrow and

* Presented at the II International Symposium on Mesic Nuclei, Kraków, Poland, September 22–25, 2013.

that a better strategy of searching for η-nuclei is required. Furthermore, the BNL experiment was in a region far from the recoilless kinematics, so that the cross section is substantially reduced [8]. More recently, the existence of η-mesic ^{3}He was claimed to have been observed in the reaction $\gamma\,^3\mathrm{He} \to \pi^0 pX$ using the photon beam at MAMI [9]. It has, however, been pointed out [10] that the data of Ref. [9] does not permit an unambiguous determination of the existence of a ^{3}Heη-bound state. The suggestion that ^{3}Heη is not bound is also supported by the theoretical studies of Refs. [11, 12].

Two different methods have been applied in the search for η bound states. One is the study of η production on nuclei and extraction of the η nucleus scattering length. The other is the direct production of the η meson in a bound state. This state is measured via missing-mass technique. The GEM Collaboration [13] has used both methods, as will be shown in this paper. This is an updated version of a talk the author has given at different occasions.

2. Searches via final state interaction

According to the Watson–Migdal theory [14, 15], when there is a weak transition to a system where there is a strong final state interaction (FSI), one can factorize the s-wave reaction amplitude, f_s, near threshold in the form

$$f_s = \frac{f_B}{1 - iap_\eta}\,, \tag{1}$$

where p_η is the η c.m. momentum and A the complex scattering length. The unperturbed production amplitude f_B is assumed to be slowly varying and is often taken to be constant in the near-threshold region.

Unitarity demands that the imaginary part of the scattering length be positive, *i.e.*, $a_\mathrm{I} > 0$. In addition, to have binding, there must be a pole in the negative energy half-plane, which requires that [11]

$$|a_\mathrm{I}|/\,|a_\mathrm{R}| < 1\,. \tag{2}$$

Finally, in order that the pole lie on the bound- rather than the virtual-state plane, one needs also $a_\mathrm{R} < 0$.

Recently, two different experiments at COSY Jülich measured η production in $pd \to \eta^3$He reactions very close to threshold with an extremely high precision of the data [16, 17].

In Fig. 1, we compare these new data with others from Refs. [16–19] in the threshold region. The width of the beam is not folded out. However, in the final analysis Mersmann *et al.* [16] did this, which is crucial for data close to the threshold. The rapid rise of the cross section close to the threshold is a clear indication of a strong final state interaction. Whereas

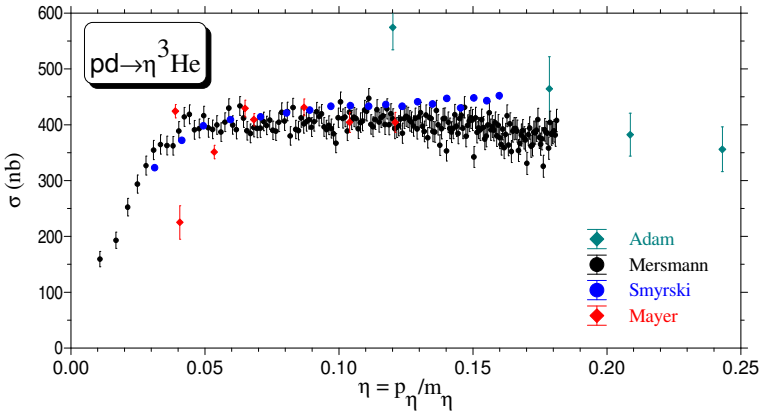


Fig. 1. Excitation function for the reaction $pd \to \eta^3\mathrm{He}$ in the threshold region as function of the dimensionless η momentum $\eta = p_\eta/m_\eta$.

Smyrski *et al.* [17] claimed that only a scattering length is sufficient to describe the data, Mersmann *et al.* [16] found a better description when an effective range is also taken into account. The result of the first group is

$$a_{^3\mathrm{He}\eta} = [\pm\,(2.9 \pm 2.7) + i\ (3.2 \pm 1.8)]\ \ \mathrm{fm}\,, \tag{3}$$

while the second group reported

$$a_{^3\mathrm{He}\eta} = \left[\pm\left(10.7 \pm 0.8^{+0.1}_{-0.5}\right) + i\ \left(1.5 \pm 2.6^{+1.0}_{-0.9}\right)\right]\ \ \mathrm{fm} \tag{4}$$

and

$$r_0 = \left[(1.9 \pm 0.1) + i\ \left(2.1 \pm 0.2^{+0.2}_{-0.0}\right)\right]\ \ \mathrm{fm} \tag{5}$$

for the effective range. Since the data are not sensitive to the sign of the real part of the scattering length, the quest for a bound state or an unbound pole cannot be answered. Its value is

$$\left|Q_{^3\mathrm{He}\eta}\right| \approx 0.30\ \mathrm{MeV}\,. \tag{6}$$

From the model calculations, it is known that binding is more probable for heavier nuclei than for lighter nuclei. We, therefore, can expect the relation

$$\left|Q_{^3\mathrm{He}\eta}\right| < \left|Q_{^4\mathrm{He}\eta}\right| \tag{7}$$

to hold. In the following, we study of the FSI of the η ^{4}He system. This is produced in the reaction

$$dd \to \eta\alpha\,. \tag{8}$$

The existing data before the GEM measurement were not sufficient to extract the s-wave contribution of the cross section. In order to do so, GEM made use of a tensor polarized deuteron beam [20]. The beam momentum of 2385.5 MeV/c corresponds to an excess energy of $Q = 16.6$ MeV for this reaction when an η-meson mass of $m_\eta = 547.7$ MeV/c^2 is used [21]. The Big Karl magnetic spectrograph [22, 23] employed for this study is equipped with two sets of multi-wire drift chambers (MWDC) for position measurement and thus track reconstruction. Two layers of scintillating hodoscopes, 4.5 m apart, led to a more accurate time-of-flight measurement than previously achieved with Big Karl. They also provided the energy-loss information necessary for particle identification. More information on the experiment are given in Ref. [20].

In a first step, the unpolarized cross section was measured. The obtained angular distribution is shown in Fig. 2. It can be fitted by Legendre polynomials. Because of the symmetric entrance channel, only even polynomials contribute. Three parameters are sufficient to reproduce the data. This indicates that there must be at least d-wave contributions. This is to be contrasted to the lower energy ANKE results [24], where $2\ell_{\max} = 2$ suffices. From the fit total cross section of $\sigma = 16.0 \pm 0.4$ nb, where uncertainties in

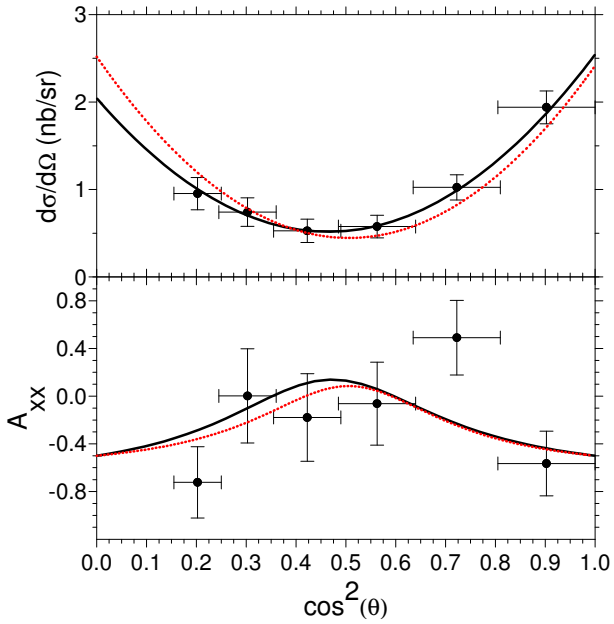


Fig. 2. Upper panel: Differential cross section for the $dd \to \alpha\,\eta$ reaction. Lower panel: Analyzing power A_{xx}. The solid curves represent a fit with four partial waves; the dotted curves with invariant amplitudes.

the target thickness, incident flux, and acceptance introduce an additional systematic error of ±1.6 nb. This value is shown in Fig. 3 together with the world data [24–26]. It seems that the cross sections start to saturate for η momenta above 80 MeV/c.

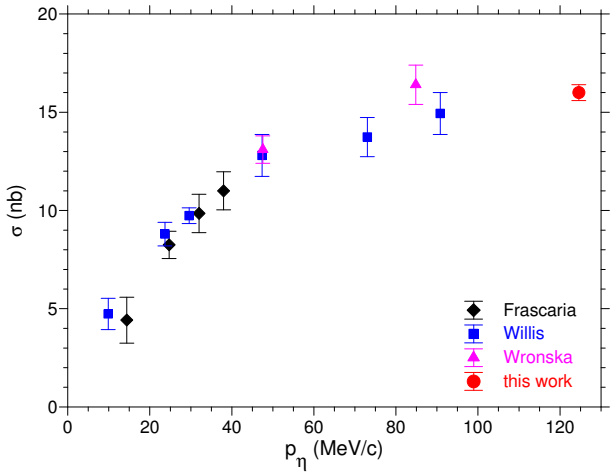


Fig. 3. Excitation function for the total cross section for the $dd \to \alpha\,\eta$ reaction. Only statistical errors are shown.

The next step is to extract the s-wave part of the total cross section. For this task, the knowledge of polarization observables is necessary. First, the polarization of the beam p_{zz} was measured by measuring elastic backward scattering of the deuterons on protons. From the known analyzing power A_{yy} the beam polarization is obtained. In the measurement of analyzing powers, one usually compares polarized and unpolarized cross sections. This introduces ambiguities because of different luminosity measurements. In order to avoid this, we applied another method. We integrated the cross section over intervals in the polar angle, where we have full geometrical acceptance of the apparatus and A_{yy} practically vanishes. We measure then only A_{xx}. The cross section integrated over these intervals of azimuthal angle becomes simply

$$I = \int\limits_{(\pi-1)/2}^{(\pi+1)/2} \left(\frac{d(\theta,\phi)}{d\Omega}\right)_{\mathrm{pol}} d\phi = \left(\frac{d\sigma}{d\Omega}(\theta)\right)_{\mathrm{unpol}} \left[1 + 0.46\, p_{zz} A_{xx}(\theta)\right] , \qquad (9)$$

where the unpolarized cross section is integrated over the same ϕ range.

Carrying out this procedure for the two polarization states, we find that

$$\Delta = \frac{I^+ - I_1^-}{I^+ + I^-} = \frac{0.23\, A_{xx}\, (p_{zz}^+ - p_{zz}^-)}{1 + 0.23\, A_{xx}\, \left(p_{zz}^+ + p_{zz}^-\right)} \tag{10}$$

and hence

$$A_{xx} = 02.44\, \Delta\,. \tag{11}$$

The angular distribution thus obtained is also shown in Fig. 2. From both angular distributions, we extract partial waves, one s-wave, one p-wave and two d-waves. This yields seven parameters to be fitted. However, strong correlations were found. An alternative method is to employ the spin structure of the matrix element. Due to the symmetry in the entrance channel, three independent scalar amplitudes are necessary to describe the spin dependence of the reaction: A, B, C. B and C have no angular dependence and for A we assume the expansion $A = A_0 + A_2 P_2(\cos\theta)$. Fortunately, the dependencies can be decoupled

$$(1 - A_{xx})\, \frac{d\sigma}{d\Omega} \;=\; \frac{p_\eta}{p_d} \left(|A_0|^2 + 2\mathrm{Re}(A_0 A_2^*) P_2(\cos\theta) + |A_2|^2\, (P_2(\cos\theta))^2 \right)\,, \tag{12}$$

$$(1 + 2A_{xx})\, \frac{d\sigma}{d\Omega} \;=\; 2\frac{p_\eta}{p_d} \left(|B|^2 \sin^2\theta \cos^2\theta + |C|^2 \sin^2\theta \right)\,. \tag{13}$$

We now extract the magnitude of the s-wave amplitude $|a_0|$. From this, we obtain a spin-averaged square of the s-wave amplitude, $|f_s|^2$ through

$$\frac{d\sigma_s}{d\Omega} = \frac{p_\eta}{p_d} |f_s|^2 = \frac{2p_\eta}{3p_d} |A_0|^2 = \frac{1}{27} \frac{1}{4\pi} |a_0|^2\,. \tag{14}$$

Wrońska *et al.* [24] could not distinguish whether the angular distribution is due to an s–p interference or a d-wave. This puzzle can be solved by our result here. The Willis *et al.* [26] data for s-wave were extracted from the measurement by just dividing by 4π. This is, however, not justified in the region of their highest point. Assuming a dependence of the d-waves with p_η^2, we can extract a more correct value for the s-wave strength. From all measurements, we then obtain a scattering length of

$$a_{^4\mathrm{He}\eta} = [\pm\,(3.1 \pm 0.5) + i\;(0 \pm 0.5)]\;\;\mathrm{fm}\,. \tag{15}$$

This result can be converted into a pole position

$$|Q_{^4\mathrm{He}\eta}| \approx 4\;\mathrm{MeV}\,. \tag{16}$$

Since the present results fulfill the conditions for a bound state — except for the sign of the real part of the scattering length — and the relation (7), it may well be that η–α binding is observed.

Searches on a more heavy nucleus were performed at SATURNE Saclay [27] and COSY Jülich [28]. Both studies employed the reaction

$$p + {}^6\mathrm{Li} \rightarrow {}^7\mathrm{Be} + \eta\,. \tag{17}$$

At Saclay, the η was measured through its two γ decay at a beam energy of 683 MeV corresponding to a momentum of 1322 MeV/c or to an excess energy of 19.13 MeV. After applying all cuts, eight events remain. They are shown in Fig. 4 and are converted into a total cross section of 4.6 ± 3.8 nb/sr or 57.8 ± 47.8 nb. Also shown in the figure are kinematical curves for ^{7}Be ground state and an excitation of 5 MeV. Clearly, the events are scattered to the whole kinematical range. ^{7}Be has in the range up to 6.73 MeV four states: two with $L = 1$, a $J = 3/2$ g.s. and a $J = 1/2$ exited state at 0.429 MeV, and two with $L = 3$, a $J = 7/2$ at 4.57 MeV and a $J = 5/2$ at 6.73 MeV. Al-Khalili *et al.* [29] have analyzed these data. They assumed that the target nucleus consists of a deuteron and an α particle. The latter acts in the reaction as a mere spectator. The cross section is then

$$\frac{d\sigma\left(p^6\mathrm{Li} \rightarrow \eta^7\mathrm{Be}\right)}{d\Omega} = \mathcal{C}\frac{p_\eta^*}{p_p^*}\left|f\left(pd \rightarrow \eta^3\mathrm{He}\right)\right|^2 \sum_J \frac{2J+1}{2}\mathcal{F}_j^2\,, \tag{18}$$

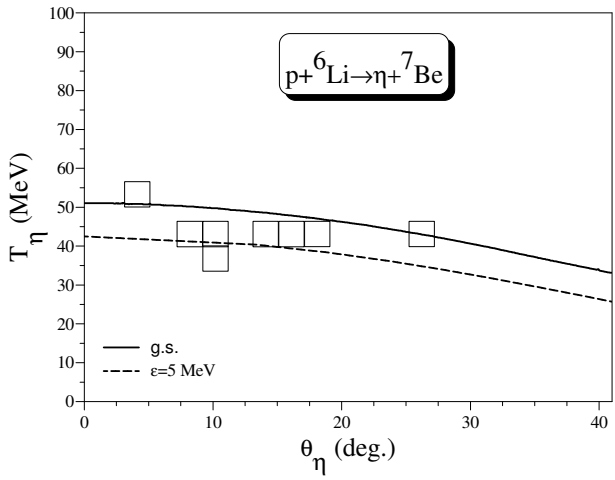


Fig. 4. The events for the indicated reaction obtained at SATURNE [27]. The solid curve is the kinematical curve for the ^{7}Be ground state, while the dashed curve is the one for an excitation of 5 MeV.

with J the total angular momentum of the final states in ^{7}Be and $\mathcal{F}_j$ their form factors. $\mathcal{C}$ is the overlap of cluster wave functions, p_η^* and p_p^* the center-of-mass momenta of the final and initial system, and $|f|$ the spin averaged matrix element of the underlying more elementary reaction $p + d \rightarrow {}^3\mathrm{He}{+}\eta$. Al-Khalili *et al.* derived the form factors from other reactions. Close to threshold, they can be assumed to be constant.

The other experiment was performed at e beam energy of 673.1 MeV, corresponding to 1310 MeV/c or an excess energy of 11.28 MeV. The recoiling ^{7}Be nuclei were detected in the spectrograph Big Karl. Since the $L = 3$ states are particle unbound, only the two $L = 1$ states contribute. The standard detectors in the focal plane were not adequate for this experiment since the recoiling particles have rather low energies of ≈ 100 MeV. The MWDC were replaced by multi-wire avalanche-chambers allowing to measure the track, followed by two layers if scintillation detectors being one meter apart. They allow particle identification via TOF measurement. All these devices were housing in a huge vacuum box made from stainless steel. The η meson events were identified via missing-mass technique. Finally, the counts were converted to cross section. The angular distribution is shown in Fig. 5. An isotropic cross section of

$$\frac{d\sigma}{d\Omega} = (0.69 \pm 0.20(\mathrm{stat.}) \pm 0.20(\mathrm{syst.}))\ \mathrm{nb/sr} \tag{19}$$

was deduced and is also indicated in the figure.

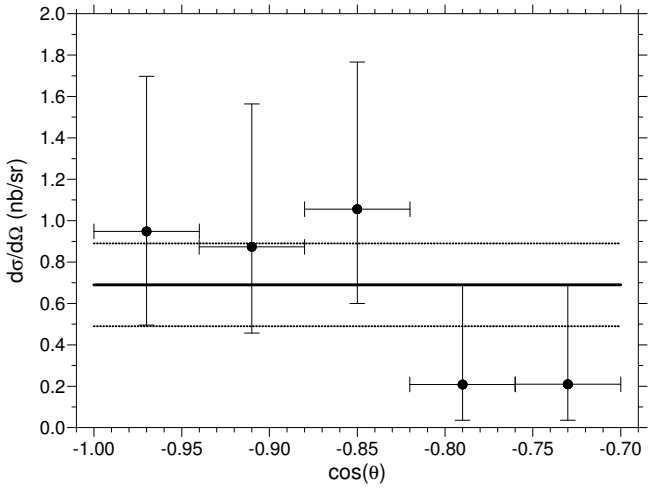


Fig. 5. Angular distribution of reconstructed η mesons [28].

Together with the formfactors from Ref. [29] and the amplitude $f(pd \to \eta^3\mathrm{He})$ extracted from the data shown above, the cross section for the ^{7}Be ground state could be extracted. The two data are shown in Fig. 6. Also shown is the energy dependence of the model normalized to the cross section of the GEM Collaboration [28], phase space dependence normalized to the same point, and model predictions [30] with and without FSI. A measurement even closer to threshold preferably below the first excited state could distinguish between the different models and could answer whether strong FSI exists in this final channel. Upadhyay *et al.* [30] got from $a_{\eta N} = (0.88 + i0.41$ fm a value $a_{\eta\mathrm{Be}} = (-9.18 + i8.53)$ fm.

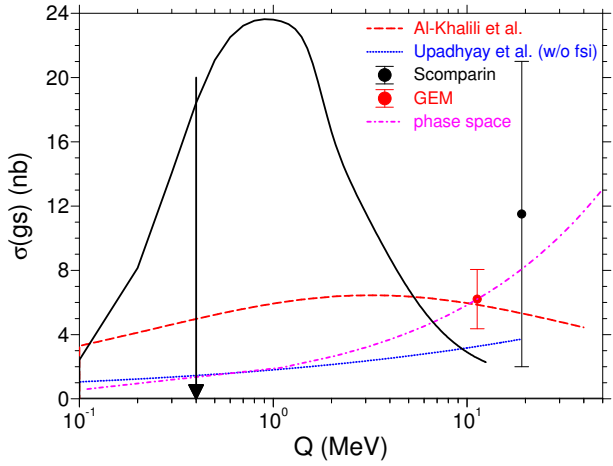


Fig. 6. Excitation function for the $p^6\mathrm{Li} \to \eta^7\mathrm{Be}$(g.s.) reaction. The two data points are from Refs. [27] and [28]. The dashed curve is the Al-Khalili *et al.* model, the dash-dotted phase space behavior, both normalized to the GEM data point. The solid and the dotted curves are calculations [30] with and without final state interactions. The arrow indicated the region where only the ground state is involved in the reaction.

3. Production of η bound nuclear states

The following method was successfully employed in the production of hypernuclei and pionic atoms. A nucleon is replaced by a hyperon or a pion. Maximal cross section is obtained when the momentum transfer from the projectile to the particle to be implanted is minimized, which means that the produced particle is almost at rest in the laboratory system. In pionic atom studies, a proton transfer via the $(d, ^3\mathrm{He})$ reaction was successfully applied [31]. However, although this reaction has reasonably large cross section it also has the disadvantage of a huge background due to the break-

up of the deuterons. The resulting protons have the beam velocity and thus the same magnetic rigidity as the ^{3}He particles. This problem can be overcome by making use of a two-nucleon transfer reaction like $(p, ^3\mathrm{He})$ but at the expense of a much smaller cross section. The choice of an odd–odd target nucleus would be ideal in order to avoid nuclear excitations as much as possible. Since there exists no solid material with these properties, ^{27}Al was chosen as a compromise. The experiment was done by making use of the following reaction chain

$$p + ^{27}\mathrm{Al} \rightarrow ^3\mathrm{He} + X\,, \tag{20}$$

where the ^{3}He carries the beam momentum away. The unobserved system X is therefore at rest. One of the possibilities is $X = ^{25}\mathrm{Mg} + \eta$. Since the η is also at rest, it can undergo a second chain of reactions

$$\eta + N \leftrightarrows N^* \rightarrow N\pi\,. \tag{21}$$

The final fate of that chain is the decay to a pion and a nucleon. In the case of a neutral resonance, the final state can be $p + \pi^-$, which have to be emitted almost back-to-back, if we ignore Fermi motion. The ^{3}He is detected with the magnetic spectrograph Big Karl [22, 23]. For the detection of the two decay particles, a dedicated detector ENSTAR was built. It has cylindrical shape around the target and consists of three layers of scintillating material. The layers were subdivided into pieces making polar and azimuthal angle measurements possible. The read-out of the pieces was performed with scintillating fibres [32]. The detector is shown during its assembling phase in Fig. 7.

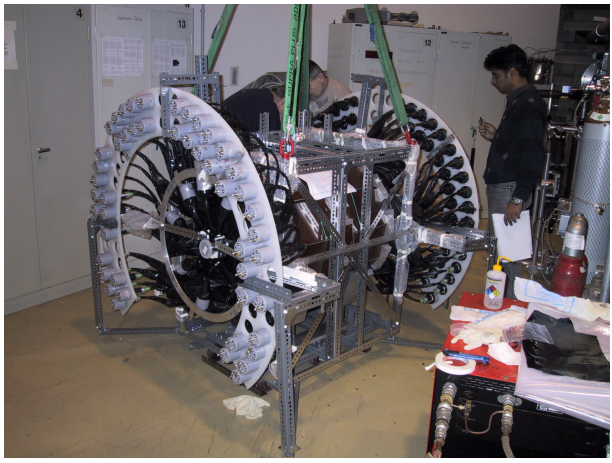


Fig. 7. The ENSTAR detector during assembling.

The experiment was performed at a beam momentum of 1745 MeV/c. At this momentum, final states with small binding energies can be produced with small momentum transfer. States with binding energies from 0 MeV to −30 MeV will have momenta below 30 MeV/c (see Fig. 8).

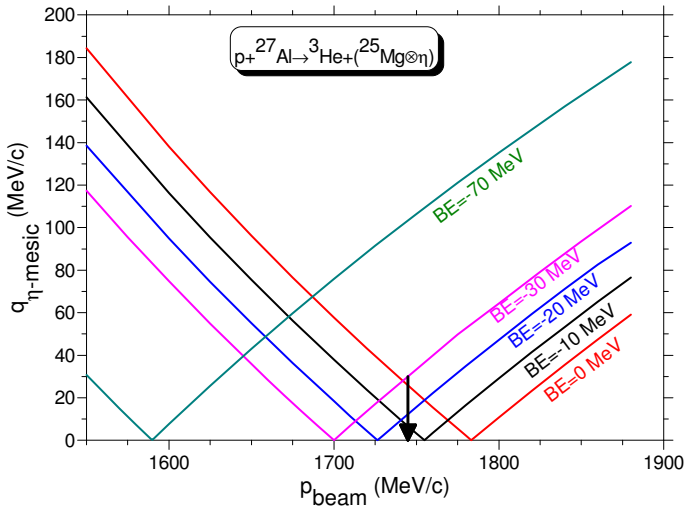


Fig. 8. Momentum transfer to the η mesic system as function of the beam momentum for the deuteron transfer reaction. The curves show the relation for different binding energies. The arrow shows the presently used beam momentum.

Two settings of the spectrograph were used with a large overlap. Excellent particle identification in Big Karl was achieved by measuring energy loss in the start detector of the TOF facility in the focal plane and TOF. In the upper panel of Fig. 9, the time-of-flight is shown without any constraint. The different bumps are due to different revolutions in the synchrotron. The needles on the third bump are from different particle species: ^{3}He, ^{3}H and ^{4}He. In the middle panel, ^{3}He are selected. The lower panel shows the spectrum when a coincidence with the ENSTAR detector is required in addition. The mean of the areas marked L(eft) and R(ight) are subtracted finally as background. In test runs, the detector elements of ENSTAR were calibrated with cosmics and reaction products from two-body reactions. It was found to be sufficient to require, in addition of the angle measurement, one particle being stopped in the middle layer, *i.e.* the proton and the second to punch through all three layers, *i.e.* the pion. Such a situation is sketched in Fig. 10. Figure 11 shows the measured missing-mass spectra. The most upper curve represents Eq. (20). Here, X can be any system excited to $\approx$ 550 MeV, but with no linear momentum. Therefore, only the requirement of a back-to-back emission of two particles is not sufficient to identify step Eq. (21). The

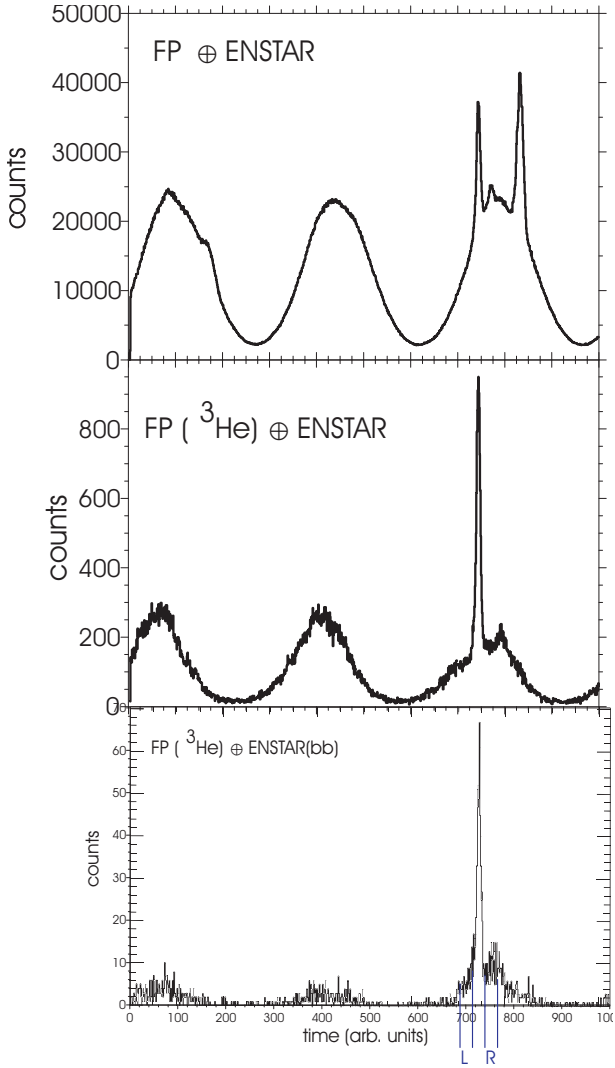


Fig. 9. The measured time-of-flight (TOF) in the focal plane of Big Karl under different boundary conditions indicated next to the appropriate spectrum.

unconstrained data do not show any structure and can be well described by a constant. For the data in the lowest spectrum, the N^* decay pattern is required. The counts are typically lower by three orders of magnitude than those in the unconstrained case and an order of magnitude compared to the case without the back-to-back requirement. Although, the $N^*(1535)$ can also decay with two-pion emission, this branch is small compared to the $p\pi^-$ channel.

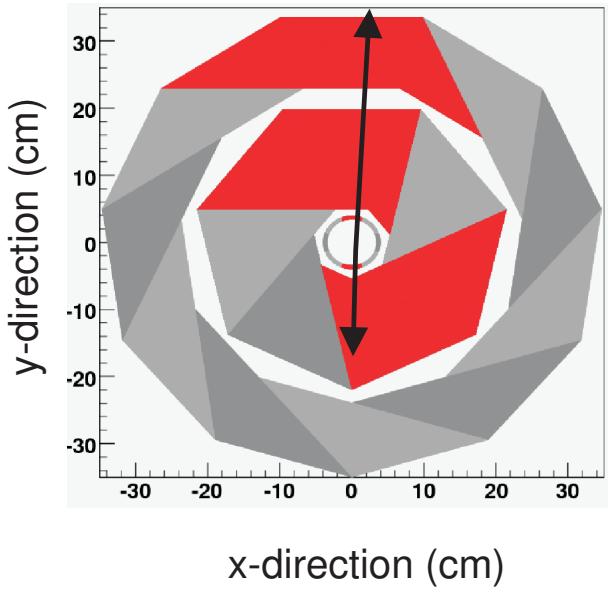


Fig. 10. Cross section of the ENSTAR detector. The arrow up indicated a pion punching through all three layers of the detector, while the arrow down indicates the associated proton being stopped in the middle layer.

The data show an enhancement around BE ≈ -13 MeV. The significance of this structure is extracted according to the two methods given in Refs. [33] and [34] respectively. At first, we test the hypothesis of peak structure being a fluctuation of background, *i.e.* the origin of the background is taken to be independent of the signal. The background outside the peak region, for simplicity approximated by a constant, was found to be 5.8 ± 0.64. The significance [33] is then given by $(N - \mathrm{BG})/\sqrt{\mathrm{BG} + \sigma_{\mathrm{BG}}}$, where N is the total counts in the region of interest, BG is the total background in this region as determined from the fit to the outside region and σ_{BG} is error in the estimation of background value as taken from the fit. This yields a value of significance which is 5.3σ. Here, we have assumed Gaussian errors. For the assumption of Poisson errors with asymmetric error bars (see Fig. 11), the background is 6.2 ± 1.0. This larger value is typical for Poisson distribution and hence the significance reduces to 4.9σ. Finally, a Gaussian on top of the background was fitted to the whole data set. This yielded for the case of Poisson statistics 6.4 ± 0.96 for the background, 8.3 ± 3.6 for the amplitude, -12.0 ± 2.2 MeV for the centroid, and 4.7 ± 1.7 MeV for the width. The corresponding curves are shown in Fig. 11. In the second method, the statistical significance is extracted by assuming the background events as well as the peak events on top of the background being Poisson distributed. Again,

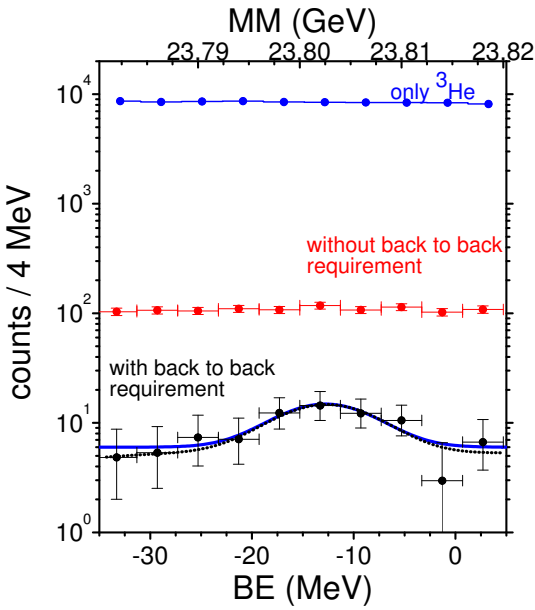


Fig. 11. Missing-mass spectra as measured with the magnetic spectrograph. The upper abscissa is the missing mass, while the lower is the binding energy of a bound system $^{25}\mathrm{Mg} \otimes \eta$ (see the text).

a constant background and a Gaussian was assumed. A fit was performed using the maximum likelihood method. The significance is then defined as, $\sqrt{-2\Delta \ln L}$. Here, $\Delta \ln L$ is the difference in the values of the logarithm likelihood function with signal fixed to zero and at the best fit value. In this way, we obtain a value of 6.20σ for the significance, assuming a simultaneous determination of amplitude, centroid and width of the signal. The fit gives for the linear background 6.38 ± 0.53 together with the values, for the signal amplitude 8.55 ± 3.05, for the centroid -13.13 ± 1.64 MeV, and for the width 4.35 ± 1.27 MeV corresponding to a FWHM of 10.22 ± 2.98 MeV. These results compare favorably with those from the first method. We, therefore, consider the present experimental results to provide a strong hint of a nuclear η bound state.

This allows us to give an upper bound for the cross section. With an estimated efficiency due to detector geometry and analysis selections of 0.70 ± 0.07, we find $\sigma = 0.152 \pm 0.054$ (stat.) $\pm$ 0.021 (syst.) nb. If this "structure" corresponds to a bound η decaying via reaction (Eq. (21)), the cross section would be 0.46 $\pm$ 0.16 (stat.) $\pm$ 0.06 (syst.) nb, assuming an isospin branching ratio of 1/3.

4. Short summary

The η production to the ^{3}Heη final state shows a dramatic rise of the cross section just above threshold. This is not seen in the heavier ^{4}Heη system. This behavior is depicted in Fig. 12. Clearly, the shapes of the excitation functions differ from each other. Since the binding probability should increase with increasing nucleon mass, this behavior does not support the existence of a bound state. On the other hand, the production experiment discussed above gives a clear signal for a bound state. The smallness of the cross section is surprising. More experiments esp. production experiments are mandatory to reach a final conclusion.

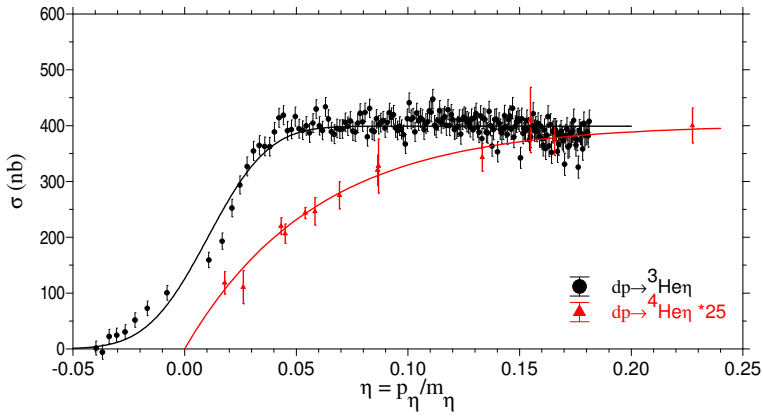


Fig. 12. Comparison of the excitation functions for the two indicated reactions. The data for the $pd \rightarrow ^3$Heη reaction are from Ref. [16], those for the $dd \rightarrow ^4$Heη reaction are given in Fig. 3. The latter data have been multiplied by a factor of 25. The solid curves are to guide the eye.

The author is grateful to the members of the GEM Collaboration. Discussions with C. Wilkin have been helpful.

REFERENCES

[1] R.S. Bhalerao, L.C. Liu, *Phys. Rev. Lett.* **54**, 865 (1985).
[2] Q. Haider, L.C. Liu, *Phys. Lett.* **B172**, 257 (1986).
[3] C. Garcia-Recio, T. Inoue, J. Nieves, E. Oset, *Phys. Lett.* **B550**, 47 (2002).
[4] R.S. Hayano, S. Hirenzaki, A. Gillitzer, *Eur. Phys. J.* **A6**, 99 (1999).
[5] K. Tsushima, *Nucl. Phys.* **A670**, 198c (2000).
[6] R.E. Chrien *et al.*, *Phys. Rev. Lett.* **60**, 2595 (1988).

[7] J.B. Lieb, Proc. International Conf. Nuclear Physics, Sao Paulo, Brazil, 1988.
[8] H. Nagahiro, D. Jido, S. Hirenzaki, *Phys. Rev.* **C80**, 025205 (2009).
[9] M. Pfeiffer *et al.*, *Phys. Rev. Lett.* **92**, 252001 (2004).
[10] C. Hanhart, *Phys. Rev. Lett.* **94**, 049101 (2005).
[11] Q. Haider, L.C. Liu, *Phys. Rev.* **C66**, 045208 (2002).
[12] S.A. Sofianos, S.A. Rakityansky, `arXiv:nucl-th/9707044`.
[13] `www.fz juelich.de/ikp/gem/`
[14] A.B. Migdal, *JETP* **1**, 2 (1955).
[15] K.M. Watson, *Phys. Rev.* **88**, 1163 (1952).
[16] T. Mersmann *et al.*, *Phys. Rev. Lett.* **98**, 242301 (2007).
[17] J. Smyrski *et al.*, *Phys. Lett.* **B649**, 258 (2007).
[18] H.H. Adam *et al.*, *Phys. Rev.* **C75**, 014004 (2007).
[19] B. Mayer *et al.*, *Phys. Rev.* **C53**, 2068 (1996).
[20] A. Budzanowski *et al.* [GEM Collaboration], *Nucl. Phys.* **A821**, 193 (2009).
[21] K. Hagiwara *et al.* [Particle Data Group], *Phys. Rev.* **D66**, 010001 (2002).
[22] H. Bojowald *et al.*, *Nucl. Instrum. Methods Phys. Res.* **A487**, 314 (2002).
[23] M. Drochner *et al.*, *Nucl. Phys.* **A643**, 55 (1998).
[24] A. Wrońska *et al.*, *Eur. Phys. J.* **A26**, 421 (2005).
[25] R. Frascaria *et al.*, *Phys. Rev.* **C50**, R537 (1994).
[26] N. Willis *et al.*, *Phys. Lett.* **B406**, 14 (1997).
[27] E. Scomparin *et al.*, *J. Phys. G* **19**, L51 (1993).
[28] A. Budzanowski *et al.*, *Phys. Rev.* **C82**, 041001(R) (2010).
[29] J.S. Al-Khalili *et al.*, *J. Phys. G* **19**, 403 (1993).
[30] N.J. Upadhyay, N.G. Kelkar, B.K. Jain, *Nucl. Phys.* **A824**, 70 (2009).
[31] T. Ymazaki *et al.*, *Z. Phys.* **A355**, 219 (1996).
[32] M. Betigeri *et al.*, *Nucl. Instrum. Methods Phys. Res.* **A578**, 198 (2007).
[33] A.G. Frodesen, O. Skjeggstad, H. Töfte, *Probability and Statistics in Particle Physics*, Universitetsforlaget, Bergen–Oslo–Tromsö 1979.
[34] R. Christov *et al.*, *Phys. Rev. Lett.* **97**, 162001 (2006).